Energy Conversion and Management 75 (2013) 532–541

Contents lists available at SciVerse ScienceDirect

Energy Conversion and Management

journal homepage: www.elsevier.com/locate/enconman

A study on heat transfer enhancement using flow channel inserts for thermoelectric power generation

Frédéric J. Lesage [a,b,*], Éric V. Sempels [c], Nathaniel Lalande-Bertrand [d]

[a] Cégep de l'Outaouais, 333 boul. de la Cité-des-Jeunes, Gatineau J8Y 6M4, Canada
[b] McMaster University, 1280 Main Street West, Hamilton L8S 4L7, Canada
[c] École Polytechnique de Montréal, 2900 Boulevard Edouard-Montpetit, Montréal H3T 1J4, Canada
[d] École de technologie supérieure, 1100 Rue Notre-Dame Ouest, Montréal H3C 1K3, Canada

ARTICLE INFO

Article history:
Received 9 May 2013
Accepted 3 July 2013

Keywords:
Thermoelectric generator
Heat transfer enhancement
Flow turbulence
Pressure drop

ABSTRACT

Thermoelectric power production has many potential applications that range from microelectronics heat management to large scale industrial waste-heat recovery. A low thermoelectric conversion efficiency of the current state of the art prevents wide spread use of thermoelectric modules. The difficulties lie in material conversion efficiency, module design, and thermal system management. The present study investigates thermoelectric power improvement due to heat transfer enhancement at the channel walls of a liquid-to-liquid thermoelectric generator brought upon by flow turbulating inserts. Care is taken to measure the adverse pressure drop due to the presence of flow impeding obstacles in order to measure the net thermoelectric power enhancement relative to an absence of inserts. The results illustrate the power enhancement performance of three different geometric forms fitted into the channels of a thermoelectric generator. Spiral inserts are shown to offer a minimal improvement in thermoelectric power production whereas inserts with protruding panels are shown to be the most effective. Measurements of the thermal enhancement factor which represents the ratio of heat flux into heat flux out of a channel and numerical simulations of the internal flow velocity field attribute the thermal enhancement resulting in the thermoelectric power improvement to thermal and velocity field synergy.

1. Introduction

The conversion of thermal energy to electricity has garnered interest in recent years due to the abundance of low cost industrial waste-heat. This resource has yet to be fully exploited for local energy needs due to efficiency limitations of the current available conversion technologies. A promising avenue for low grade waste-heat recovery stems from the Seebeck effect in which an electromotive force is generated by a thermal dipole across a semiconductor. The current difficulties in applying this phenomenon pertain to the thermoelectric conversion efficiency which limits the cost effectiveness of the technology. The ongoing efforts to improve thermoelectric conversion efficiency may be grouped into three categories: (1) material conversion efficiency; (2) thermocouple design efficiency; and (3) thermal system efficiency.

In the material conversion efficiency category, the capacity of thermoelements to generate an electromotive force from a thermal dipole is investigated. This thermoelectric phenomenon is quantified in terms of the dimensionless Figure-of-Merit *ZT* [1] which is a function of temperature, electrical conductivity, thermal conductivity and the Seebeck coefficient (ratio of carrier's transported entropy to its charge); the greater the Figure-of-Merit the greater the material's thermoelectric conversion efficiency. For a temperature range below 450 K, commercially available materials with a Figure-of-Merit greater than unity are based on the alloy bismuth (Bi) combined with antimony (Sb), selenium (Se), and tellurium (Te) [1]. In an effort to improve material thermoelectric efficiency, many studies such as those of André et al. [2] and Poudeu et al. [3] aim to engineer materials with higher Figure-of-Merit values for target temperature ranges by investigating different alloy combinations and different compositions. Thermocouple design efficiency studies such as those of Ebling et al. [4] and Hadjistassou et al. [5] investigate improvements to module performance. This was done with geometrical investigations and segmented pellet leg investigations in an attempt to enhance charge carrier concentration.

The heat transfer efficiency of the thermal system maintaining the thermal dipole dictates the thermoelectric conversion potential of the device. For this reason, thermal system efficiency studies investigate the heat flux in and out of the system in an effort to

* Corresponding author at: Cégep de l'Outaouais, 333 boul. de la Cité-des-Jeunes, Gatineau J8Y 6M4, Canada. Tel.: +1 819 770 4012; fax: +1 819 770 8167.
E-mail addresses: Frederic.Lesage@cegepoutaouais.qc.ca (F.J. Lesage), eric_sempels@hotmail.com (É.V. Sempels), nathanielbertrand@gmail.com (N. Lalande-Bertrand).

0196-8904/$ - see front matter © 2013 Elsevier Ltd. All rights reserved.
http://dx.doi.org/10.1016/j.enconman.2013.07.002

Nomenclature

Symbol	Description
c_p	specific heat at constant pressure (J/kg K)
n	number of channels (–)
p	pressure (PSI)
P	power (W)
P^*	P_i/P_o (–)
P^+	$P^* - \dot{W}_{\Delta p}/P_o$ (–)
q	heat transfer rate (W)
r	radial axis (m)
R_L	electrical load resistance (Ω)
T	temperature (K)
$\dot{V}$	volumetric flow rate (m^3/s)
$\dot{W}_{\Delta p}$	pumping penalty (W)
x	central channel axis (m)

Greek letters

α	Seebeck coefficient (V/K)
ρ	fluid density (kg/m^3)
η	q_i/q_o (–)
τ_r	shear stress (N/m^2)

Subscripts

C	cold side (–)
H	hot side (–)
i	flow with inserts (–)
in	inlet (–)
o	flow without inserts (–)
out	outlet (–)

maximize the temperature gradient across its embedded thermoelectric modules. The aim of these studies varies depending on the particular heat sources and heat sinks that are available. For the most part, thermal efficiency system studies consider a low-cost low-grade heat source [6,7,8] and aim to maximize the power output of commercially available thermoelectric modules by minimizing the pumping penalty of the heat sink. Bismuth Telluride (Bi_2Te_3) modules are common in thermal system studies [9,10,11] since they have been identified by Karabetoglu et al. [12] (among others) as the most efficient thermoelectric module for low-cost heat sources within the temperature range of 273–473 K. For example, [13–17] investigated thermoelectric system efficiency using vehicle heat exhaust, O'Shaughnessy et al. [18] harnessed thermoelectric power from biomass cook stove residual heat, [19–22] proposed thermoelectric systems exploiting solar radiation, [23–25] investigated system efficiency of a thermoelectric conversion of excess heat of a photovoltaic panel, and many studies such as [26,27,28,29,30,31,32] investigated flow channel thermoelectric systems for industrial Waste-heat recovery applications. Many industrial liquid-to-liquid heat exchangers are commonly used for expelling excess heat from the working instruments and operating environment for production and security needs. Such heat exchangers offer a thermal system that could potentially maintain a thermal dipole for thermoelectric power production if the gain in power can offset the pumping penalty that results from the presence of the generator. In this way, a liquid-to-liquid thermoelectric generator which achieves the necessary efficiency to offset the pumping penalty would contribute to the industry's local electrical energy needs.

The present work studies thermal enhancement in a liquid-to-liquid thermoelectric generator resulting in an increase in the thermal dipole thereby increasing the charge carrier concentration in the embedded Bi_2Te_3 materials. The method of investigation considers flow channels fitted with turbulating inserts of different geometry and under varying thermal input conditions. The ability for the inserts to enhance heat transfer by way of field synergy and their ability to enhance thermoelectric power sufficiently to offset the adverse pressure drop are measured and discussed.

1.1. Thermoelectric power

Thermoelectric power is a result of the thermoelectric phenomenon in which a charge carrier in an electrical conductor is mobilised once subject to a thermal field maintaining a thermal dipole across the conductor. In order to create a circuit, the chosen conductor is separated into thermoelements that are either doped to favour positive charge carrier mobility (p-type) or negative charge carrier mobility (n-type). The thermoelements are then placed in an alternating series in the thermal field in order to circulate an electric current. A p-type thermoelement and an n-type thermoelement pair constitutes a thermocouple. As previously discussed, conversion efficiency may be investigated by the materials and by the module design for greater charge carrier concentration and less thermal conduction across the module. The present study however investigates methods for managing the thermal field that is maintaining the thermal dipole responsible for generating the electromotive force. More specifically, as illustrated in Fig. 1, a heat flux from a heat source to a thermoelectric module and a heat flux from the module to the heat sink are necessary and represent a critical step in system thermoelectric conversion efficiency. This is due to the fact that thermoelectric power sensitively increases in efficiency with an increasing temperature dissimilitude across the conductor elements. Indeed, Hodes [33] demonstrated that the maximum power output of a single thermocouple is proportional to the square of $\Delta T = T_H - T_C$ in which T_H is the hot side temperature and T_C is the cold side temperature such that for a single thermocouple,

$$P = \frac{(\Delta T \alpha)^2}{4R_L} \tag{1}$$

In Eq. (1) α is the material Seebeck coefficient and R_L is the electrical load.

System efficiency of thermoelectric applications therefore pertains to maximizing the thermal transport from the available heat source to the surface of the hot side of the thermoelectric module. Similarly, the thermal system seeks to increase efficiency by optimizing the thermal transport from the cold side of the module to the available heat sink.

In the present study, the thermal transport enhancement brought upon by turbulating inserts in a liquid-to-liquid generator with embedded thermoelectric modules is investigated. The heat source is hot water in a flow channel at a constant flow rate and the heat sink is cold water in a flow channel at a constant flow rate.

2. Experimental setup

2.1. Test stand

A test stand is built in order to measure the influence of different flow turbulence characteristics on thermoelectric power

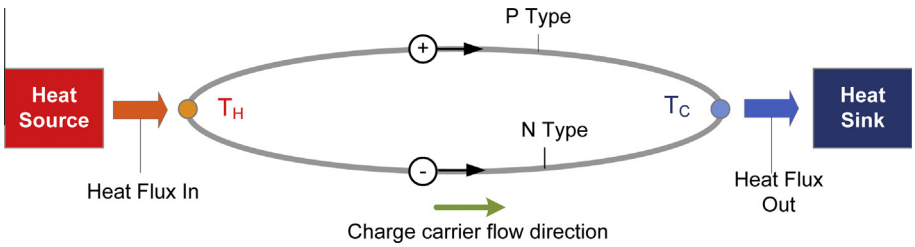

Fig. 1. Thermoelectric circuit from a thermal dipole.

output. To this end, each of the two thermoelectric liquid-to-liquid test generators is fitted with removable flow turbulating inserts. The test stand channels hot and cold water to the generator in order to create a temperature gradient across embedded thermoelectric modules (TEMs). The experimental setup, illustrated schematically in Fig. 2, consists of a thermoelectric generator (TEG), a hot water circuit, a cold water circuit and an electrical circuit such that the TEG operates thermally in parallel and electrically in series. It is important to note that the load resistance used for the electrical circuit has a value of 1 Ohm, that the temperature reading for the cold flow inlet is prior to the channel division and that the temperature reading for the cold flow outlet is after the channel fusion.

2.2. Liquid-to-liquid thermoelectric generators

Each TEG has two sets of commercially available TEG2-07025HT-SS TEMs connected in series into two layers. Each of these layers are embedded between a cold and a hot aluminum plate for a total of three aluminum plates as shown in Fig. 3. This results in two aluminum encased purpose built thermoelectric liquid-to-liquid generators assembled by Thermoelectronics Corp.

Each TEM is composed of alternating p-type and n-type semiconductor pellets of bismuth telluride (Bi_2Te_3) connected in series and held in place by thin ceramic plates. A p-type pellet leg is a semiconductor element which has been doped to favor positive charge carrier mobility. Conversely, n-type legs favor negative

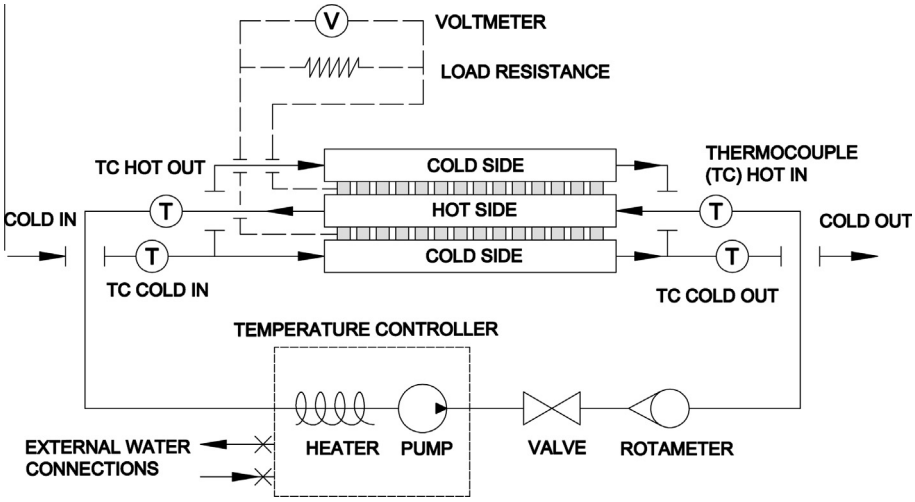

Fig. 2. Schematic representation of the experimental setup: water circuit, electric circuit and thermoelectric generator.

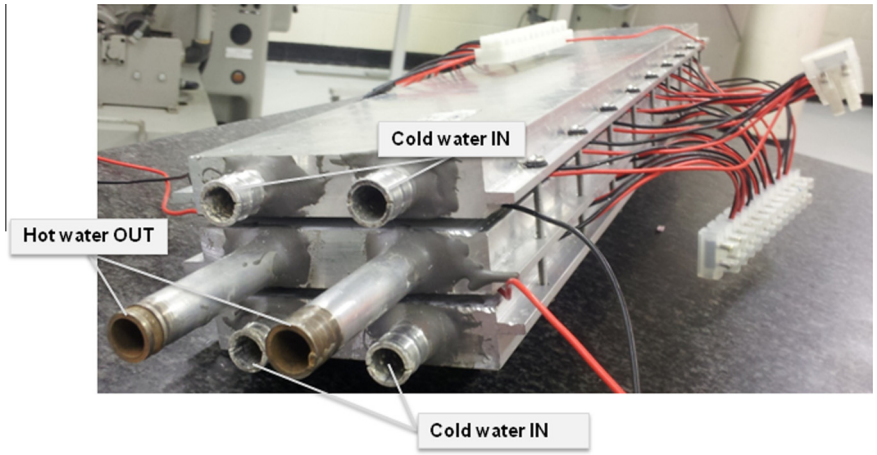

Fig. 3. Presentation of the fluid inlets and outlets of the thermoelectric generator TEG40.

charge carrier mobility. The electromotive force created by the thermal dipole mobilizes the charge carriers to flow from the hot end to the cold end of each pellet leg. By alternating the pellets, an electric current is maintained through the p–n junctions. Each of these modules measures 30 mm × 30 mm × 4.8 mm. A full description of the thermal profile and the thermoelectric conversion process of an individual TEM is provided in Lesage and Pagé-Potvin [32]. The two generators used in the present study are designated TEG8 and TEG40 referring to the number of TEMs contained in each one. Dimension specifications of the two generators are presented in Table 1.

Each of the aluminum plates of each generator contains two parallel channels each of which having an inner diameter of 9.52 mm and an outer diameter of 12.70 mm. In order to minimize thermal interaction with the ambient environment, each generator is isolated in machined Styrofoam. For protective purposes from possible hot water hazards, the entire device is enclosed in a Plexiglas box during generator operation.

The hot water temperature is regulated by a MicroTherm CMX Series Temperature Control System which effectively combines the pump and the closed loop heating unit. The cold and hot water temperatures are measured using type *T* thermocouples in which data acquisitioning is made possible with an Omega interface of ±0.1 °C tolerance. The flows for each test case are controlled using rotameters.

It is important to note that the hot and cold water flow are in opposing directions. This is done purposefully in order to favour a more homogenous thermal profile through the generator. Indeed, the TEMs are connected in series inside the generator and thus a comparatively low temperature gradient across one module will have an impact on the electromotive force driving the electrical current of the entire series.

2.3. Power output measurements

In the electric circuit illustrated in Fig. 2, the voltage is measured at the load resistance using a ScienceWorkshop 750 interface. Pasco's DataStudio is used for data acquisition of the real time calculation of the electrical current, voltage and power production. For the 0.4–3.0 V voltage range of this study, these instruments provide voltage measurements within an uncertainty of ±3 mV. Therefore, for the voltage range of this study, the uncertainty in the voltage readings range from ±0.1% to ±0.75%. Vishay, the maker of the fixed wirewound load resistance R_L of this study, ensures that the load has a value of 1 Ω with a tolerance of 1%. From circuit theory, the resultant power output measurements therefore have a range in uncertainty of ±1.2% to ±2.5%. The voltage and temperature measurements are taken every 10 s for a period of 5 min and averaged over this interval for each test case.

2.4. Flow turbulating inserts

The parameter targeted by this study is the effect of modified turbulence on the power production of a thermoelectric generator. For the working conditions of the considered test cases, the flow is maintained within the turbulent regime as confirmed by Reynolds number calculations that are greater than 2300 for water flow rates varying from 1.25 l/min to 4 l/min per 9.52 mm inner diameter channel at temperatures ranging from 20 °C and 90 °C. The Reynolds number is calculated as the ratio of the inertia to the viscous forces in which the characteristic length for internal pipe flow is the inner diameter of the pipe [36]. For the given working conditions, the Reynolds numbers range from 2900 to 28,070 placing all test conditions of this study in the turbulent regime.

In order to enhance the heat transfer at the channel walls for flows that are within the turbulent regime, three different types of inserts were designed and manufactured for this study. They are each made from 0.51 mm thick cooper sheets that are cut 8.3 mm in width and are long enough to run the entire length of each channel. The turbulating inserts are referred to in the present text as: the Spiral Insert, the 16 mm Panel Insert, and the 8 mm Panel Insert and are presented in Fig. 4. Each of the Spiral Inserts is twisted along its length pitch to one revolution per 10 cm. The 16 mm Panel Inserts and the 8 mm Panel Inserts have 4 mm panels punched through them in alternating direction every 16 mm and 8 mm respectively. The Panels are at approximately 110° with the horizontal relative to point of flow entry.

2.5. Pressure drop

Heat transfer enhancement associated with internal flows can be made possible by introducing surface roughness [34] or flow impeding obstacles [35] effectively increasing the convection coefficient. By introducing the flow turbulating inserts a secondary flow is created generating local heat transfer coefficients at the periphery of the flow channel [36]. It is well illustrated by Tijing et al. [37] that the heat transfer enhancement by way of flow channel inserts necessarily increases the pressure drop resulting in a pumping penalty. For the experimental conditions of the present study, the entry length for the turbulent flow with turbulating inserts is considered independent of the Reynolds number and approximately 10 times the inner radius of the channel. This is considered a safe estimate since the flow entry path is divided into two entry regions by the inserts and it is standard practice to assume the entry length for the fully developed turbulent flow to by ten times the diameter of the flow entry cross section and for it to be Reynolds number independent [36]. For this reason, the generator's pipes extend out in order to attain the entry length needed for fully developed turbulent flow prior to the location in which heat is transferred to the embedded TEMs. Indeed, by considering the net momentum flux in the fully developed region of the pipe, the conservation of momentum dissolves to a force balance between the pressure and shear forces,

$$r\frac{dp}{dx} = -\frac{d}{dr}(r\tau_r) \tag{2}$$

Table 1
Specifications of the generators.

	Length (mm)	Width (mm)	Height (mm)	# of TEMs
TEG8	125.0	90.0	17.3	8
TEG40	472.0	90.0	17.3	40

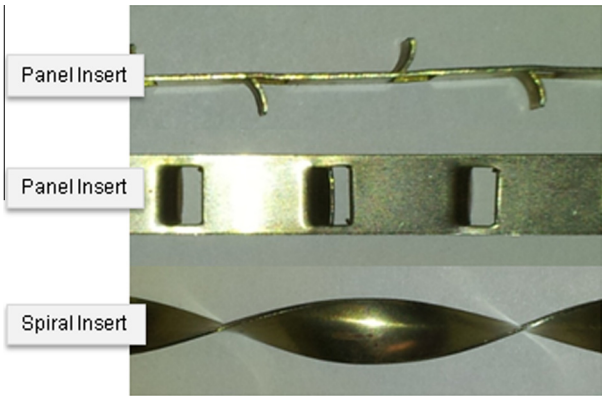

Fig. 4. Removable flow turbulating inserts.

in which r is the radial axis, x is the central axis, p is the internal pressure and τ_r is the shear stress. The increase in pressure drop associated with turbulating inserts impeding the flow is therefore attributed to the increase in available area for which shear stress can manifest itself inside the flow channel. Furthermore, the surface tension at the periphery of the channel can be increased by flow altering obstacles which increase the velocity gradient at the surface.

The goal of this study is to measure the thermoelectric power gain due to heat transfer enhancement relative to the increased work done due to the associated pressure drop. To this end, a second test stand, illustrated in Fig. 5, is built for precision measurements of pressure drops resulting from a flow turbulating insert inside. It is important to note that in the experimental setup schematically represented in Fig. 5, an individual flow channel of equivalent material and geometrical design to that of the TEG40 generator pipes is used to measure the adverse pumping penalty due to the presence of a turbulating insert. The pressure drop in the pipe before and after placing the insert is measured for a fixed flow rate. The added power to the system necessary to counter the increased pressure drop due to a flow turbulating insert is calculated as,

$$\dot{W}_{\Delta p} = n(\Delta p_i - \Delta p_o)\dot{V} \tag{3}$$

in which n is the number of channels, Δp_i and Δp_o are the pressure drops with and without the flow turbulating inserts respectively and $\dot{V}$ is the volumetric flow. It is important to note that in the present study, there are six channels for each of the test cases. Furthermore, under operating conditions with inserts all six channels are fitted with equivalent inserts.

This uncomplicated test stand controls the mean pressure inside the TEG while measuring the pressure at the channel inlet and outlet with a 0.1 PSI tolerance using an Omega DPG1001B-100G High-Accuracy Digital Pressure Gauge. The flow rates are controlled using a spring and piston flow meter with a 2% tolerance. It is important to note that the variation in pressure drop due to a variation in fluid temperature is measured to be within the uncertainty of the measuring instruments of this study. For this reason, the pressure drop relative to the channel insert is considered independent of fluid temperature for the thermal conditions tested.

3. Results and discussion

3.1. Insert performance comparison

The TEG8 generator is tested over a range of thermal input conditions without any inserts using a flow rate of 2.5 l/min per channel. The tests are repeated fitting the generators channels with 16 mm Panel Inserts, 8 mm Panel Inserts and Spiral Inserts. It is important to note that inserts are either absent from all channels or of the same configuration in all channels for each test case.

In order to evaluate the generator's performance relative to the thermal operating conditions, the output is measured with respect to ΔT. Due to the fact the present work builds upon that of Lesage and Pagé-Potvin [32], for comparative purposes an equivalent ΔT definition is used here such that,

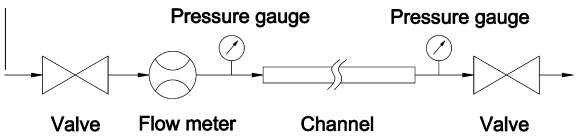

Fig. 5. Pressure drop measurement setup.

$$\Delta T = \left(\frac{T_{in} + T_{out}}{2}\right)_H - \left(\frac{T_{in} + T_{out}}{2}\right)_C \tag{4}$$

in which T_{in} and T_{out} are the outlet and inlet temperatures respectively.

It is observed in Fig. 6 that amongst these inserts, the greatest thermoelectric power performance is obtained using the 8 mm Panel Inserts. The results show a minimal power increase when operating with Spiral Inserts in the flow channels and an important power increase when operating with Panel Inserts. This observation is in agreement with Tijing et al. [37] who showed negligible heat transfer enhancement when using twisted fin configuration inserts in a counter-flow heat exchanger. Furthermore, the results show a power output exponential growth curve relative to ΔT. This implies that for increment increases in ΔT in the lower temperature range, there is a smaller thermoelectric power increase than that which is obtained with increment increases in ΔT in the upper temperature range.

3.2. Thermoelectric power enhancement

In an effort to compare the power enhancement of the different turbulating inserts, the power production associated with each insert is normalized by the power production attained in an absence of any inserts such that,

$$P^* = \frac{P_i}{P_o} \tag{5}$$

in which P_i is the enhanced thermoelectric power with inserts and P_o is the measured power without inserts.

From the results presented in Fig. 6, second order polynomial curve fits are used to evaluate the thermoelectric power enhancement of each insert. The results of this analysis for all of the thermal input conditions tested on the TEG8 generator for a 2.5 l/min flow rate per channel are presented in Fig. 7. It is important to note that unity implies zero power enhancement relative to an absence of inserts.

The results illustrated in Fig. 7 show that the greatest thermoelectric power enhancement amongst the tested conditions is attained when fitting the flow channels with 8 mm Panel Inserts and that the minimum is attained when using the Spiral Inserts.

It is important to note that the 8 mm Panel Inserts have 100% more panels than the 16 mm Panel Inserts while performing only marginally better with respect to power output gain relative to an absence of inserts. This suggests that there is an optimal pitch after which adding panels would cause more restriction in the flow than benefit in generated power. The existence and localization of

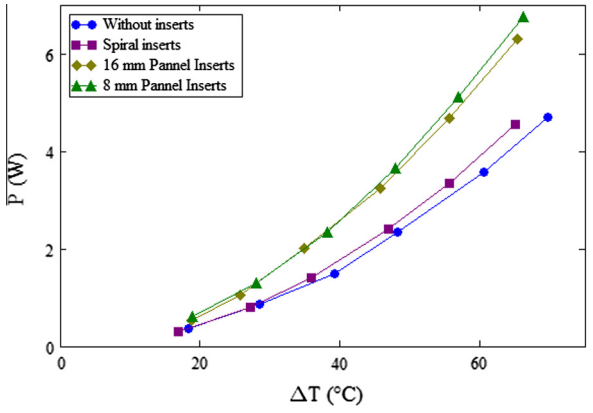

Fig. 6. TEG8 thermoelectric power production using different flow turbulating inserts and a 2.5 l/min flow rate per channel.

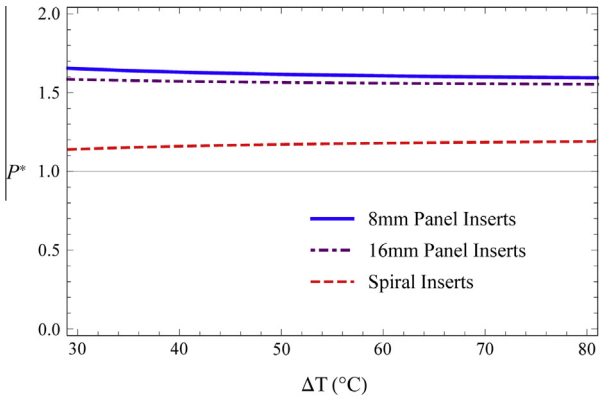

Fig. 7. Normalized thermoelectric power output of TEG8 using different flow turbulating inserts and a 2.5 l/min flow rate per channel.

this optimal pitch as well as the effect of varying volumetric flow rate are the object of a future study.

3.3. Thermal enhancement

The power enhancement observed in Section 3.2 is attributed to enhanced heat transfer brought upon by the presence of turbulating inserts in the flow channels. Indeed, the increase surface generates swirling and secondary flows interrupting the thermal boundary layer development. More specifically, the secondary flow effectively prevents thermally fully developed flow inside the channels. This is attributed to secondary flows decreasing the thermal boundary layer near the surface and effectively increasing the radial temperature gradient thereby increasing the heat flux at the periphery of the flow channel.

The effect of the presence of the turbulating inserts on the heat transfer rate q out of the hot flow channel and into the cold flow channel are measured from the simplified steady-flow thermal energy equation,

$$q = \dot{V}\rho c_p(T_{out} - T_{in}) \tag{6}$$

in which ρ and c_p are the density and the specific heat respectively of the working fluid.

In order to generate precise results, the TEG40 generator is used to evaluate the heat transfer rates. This is due to its longer channels yielding greater heat transfer rate and decreasing the percentage uncertainty in the measurements. In this way, the 0.1 °C uncertainty in the measuring instruments is negligible compared to the temperature drop of the hot channel or the temperature rise of the cold channel from inlet to outlet.

Fig. 8 compares the heat transfer rates in the presence of 8 mm Panel Inserts and in an absence of inserts. The flow rate is maintained at 2.5 l/min for all test cases and the thermal input conditions are varied. In the calculation of the heat transfer rates, the values of the fluid characteristics such as density and specific heat are taken with respect to the average channel temperature using the thermophysical properties provided in Incropera et al. [36]. The results are presented in Fig. 8 showing an increase in heat transfer rate for both the cold and hot flow channels when 8 mm Panel Inserts are used relative to an absence of inserts. In Fig. 8, q_i and q_o denote the heat transfer rates with and without inserts respectively for the hot and cold flow channels. The cold side heat transfer is shown to be less significant than that of the hot side. This is attributed to the fact that the cold fluid flow is closer to the ambient air temperature implying that a more significant portion of the measured heat transfer from the hot side is due to thermal diffusion into the local environment.

The thermal enhancement brought upon by the presence of the turbulating inserts is measured by way of the thermal enhancement factor η. The thermal enhancement factor has been defined by Tijing et al. [37] as the ratio of the enhanced (due to surface roughness or turbulating inserts) convection coefficient h_i to the convection coefficient of a smooth surface free of flow impeding inserts h_o. In the present study, the thermal enhancement factor is measured as the ratio of the heat flux out of the flow channel with insert to the heat flux out of the flow channel without insert. Using the simplified steady-flow thermal energy equation, the enhancement factor is defined here as,

$$\eta = \frac{q_i}{q_o} \tag{7}$$

From the results presented in Fig. 8, second order polynomial curve fits are used to evaluate the thermal enhancement factor of the 8 mm Panel Inserts. Fig. 9 illustrates the thermal enhancement factor evolution with respect to ΔT for the hot and cold channels as well as the thermoelectric power enhancement. For low ΔT value's, the hot channel thermal enhancement factor is less than unity corresponding to a thermal transport impedance due to the presence of the 8 mm Panel Inserts. This is offset however by a cold channel thermal enhancement factor that is greater than unity. The combined result for low ΔT values is a power enhancement factor that is greater than unity. For larger ΔT values, both the hot channel and cold channel thermal enhancement factors increase sharply to a maximum and decrease more gradually beyond the maximum. Similarly, the power enhancement factor is observed to increase more sharply for lower ΔT values attaining a maximum of more

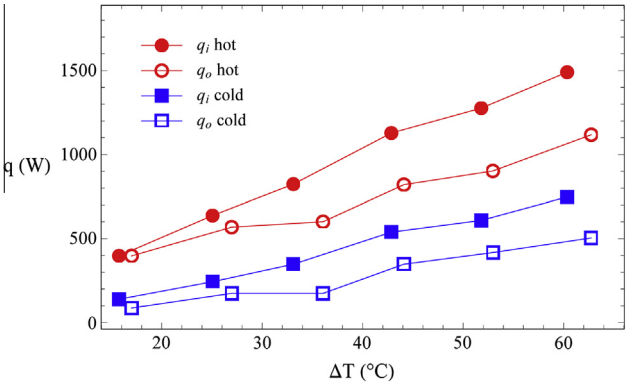

Fig. 8. Heat transfer rate of the hot and cold flow channels with and without the 8 mm Panel Inserts.

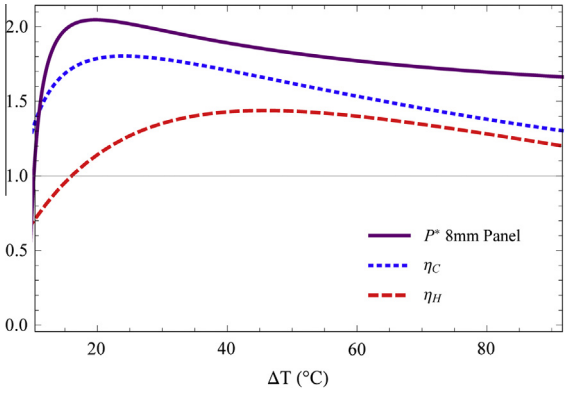

Fig. 9. Thermal enhancement and power enhancement due to the 8 mm Panel Inserts in the TEG40 at 2.5 l/min per flow channel.

than 110% improvement from the power obtained without inserts. Beyond the maximum, the power enhancement evolution with respect to the thermal input conditions decreases steadily. More importantly, the thermal power enhancement factor is measured to be above unity for the range of thermal input conditions tested.

The results of Fig. 9 are significant in that they illustrate maximum thermal enhancement conditions for the flow in the presence of an 8 mm Panel Insert. In particular, the maximum thermal transport enhancement of the cold and hot flow rates are attained at ΔT values of 24.1 °C and 45.7 °C respectively. This implies that there are optimal thermal input conditions associated with the maximum thermal enhancement attainable by Panel turbulating inserts. It is important to note that the TEG40 used to generate Fig. 9 is larger and produces more power than the TEG8 used to generate Fig. 7. The relative sensitivity of inserts on thermal and power enhancement is therefore more detectible with the larger of the two generator. Indeed, the evolution curve with respect to thermal conditions illustrated in Fig. 9 more closely adheres to that which is expected: a sharp rise from no enhanced power for a near zero thermal dipole converging to a stabilized value for greater thermal input conditions.

Fig. 10 represents the evolution of the rate of change of the thermal enhancement factor with respect to ΔT and the rate of change of the thermoelectric power enhancement with respect to ΔT for 2.5 l/min flow per channel in the presence of 8 m Panel Inserts in the TEG40. It effectively illustrates the evolution of the slope of the thermal and power enhancement curves presented in Fig. 9. It shows that in the presence of Panel Inserts, increasing the thermal input conditions for low ΔT values improves thermal transport and thermoelectric power generation and that increasing the thermal input conditions for higher ΔT values decreases the enhancements. The rate of change with respect to ΔT is shown to converge to near zero negative values in the upper temperature range for the power enhancement and for the thermal enhancement factors indicating a more gradual linear decrease in the evolution curves as the temperature rises in this upper range.

To summarize, the results show that the enhancement at low ΔT values is sensitive to small changes in temperature. Conversely, for larger ΔT values, the rate of change becomes near constant and near zero implying a stability in the thermal and power enhancement brought upon by the 8 mm Panel Insert and that the thermal and power enhancements are less sensitive to changes in thermal conditions for the upper temperature range.

3.4. Velocity field

The thermoelectric power enhancement is primarily attributed to the increase of velocity near the channel wall resulting in a minimized boundary layer and a change in the velocity profile. More specifically, turbulating inserts enhance thermal transfer by increasing the velocity gradient near the periphery. Indeed, heat transfer is optimized in channel flow once synergy is obtained between the velocity vector and the temperature gradient. This is known as the field synergy principle [38,39] which states that the heat transfer in a channel is maximized when the angle between the directional vectors is minimized. Indeed Ma et al. [40] demonstrates experimentally and Kuo et al. [41] demonstrates numerically that an interruption in flow induced by impeding obstacles results in a reduced angle between the velocity vector and the temperature gradient thereby enhancing heat transfer.

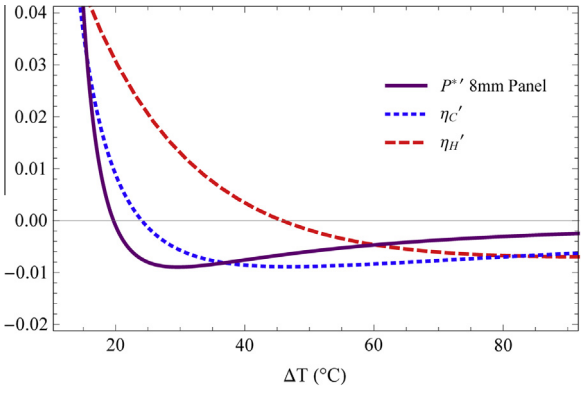

Fig. 10. Rate of change of the thermal enhancement of the 8 mm Panel Inserts of the TEG40 at 2.5 l/min per flow channel.

Since the thermal transport from the fluid channel of this study to its surrounding generator is perpendicular to the mean flow direction, the field synergy principle effectively implies that thermal transport is enhanced if the velocity vector is adjusted to a more perpendicular direction relative to the mean flow. In order to analyze the velocity field in the channels, the flow is simulated using a standard k-epsilon model with Autodesk Simulation CFD software. It is based on the turbulent kinetic energy (TKE) and turbulent energy dissipation (TED) equations which was shown to predict the diversity of turbulent flows both near and remote from the channel walls by Jones and Launder [42]. The simulations are run inputting the physical properties of aluminum alloy 6061 and water as the working material and fluid respectively. These working conditions are input for a an inlet temperature of 40 °C and an inlet flow rate of 2.5 l/min resulting in a 0.585 m/s inlet velocity and a Reynolds number of 8753 placing the flow within the turbulent regime. The gauge pressure at the outlet is set to 45 PSI providing a boundary condition and all simulations are run assuming Steady State conditions. The simulations are computed running a minimum of 200 iterations with boundary conditions of velocity at the flow channel inlet and pressure at the flow channel outlet.

Fig. 11 illustrates the internal longitudinal fluid velocity in the presence of an 8 mm Panel Insert, in presence of a Spiral insert and in absence of any insert. The simulations show that the magnitude of the velocity is less uniform in the presence of the 8 mm Panel Insert such that the longitudinal velocity component is minimal near the central axis and attains a maximum near the periphery. In contrast, in absence of any insert, the velocity field is more uniform throughout the channel and the velocity profile is maximal near the central axis. It is also shown in Fig. 11 that the mean velocity field profile alterations due to the Spiral Insert are negligible implying negligible thermal transport enhancement. However, in the presence of the 8 mm Panel Insert, the increase in the longitudinal velocity component near the surface is due to a velocity vector that is made more perpendicular to the mean flow sending a greater volume of fluid to the periphery. Since the channel flow rate is maintained, this results in an increase in the local longitudinal velocity component near the wall.

To summarize, the results of Fig. 11 confirm the observations of Section 3.3 in showing that the 8 mm Panel Inserts better enhance thermal transport than the Spiral Inserts relative to an absence of inserts. Indeed, it is shown that the field synergy principle is less satisfied in the presence of the Spiral Inserts since the longitudinal velocity component is less augmented than is observed in the presence of the 8 mm Panel Inserts. The increased velocity near the surface is attributed to a volume flux through a smaller portion of the channel deviated by the insert thereby changing the velocity profile and in particular increasing the longitudinal velocity component near the wall. The redirected velocity vector becomes more perpendicular to the mean flow and, by the field synergy principle, thermal transport near the surface is increased.

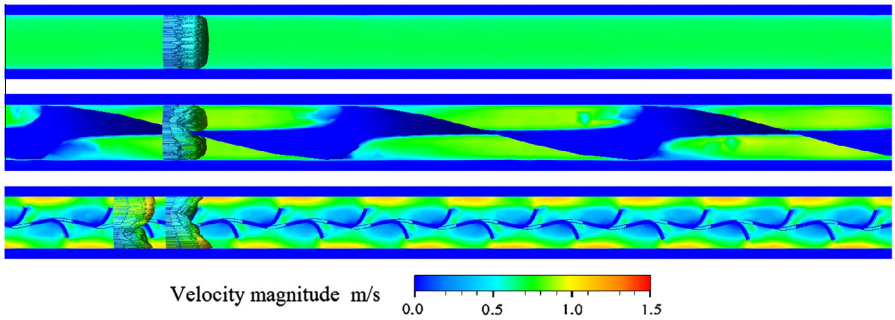

Fig. 11. Comparison of the longitudinal velocity profile in flow channels: (left) 8 mm Panel Insert; (right) absence of inserts.

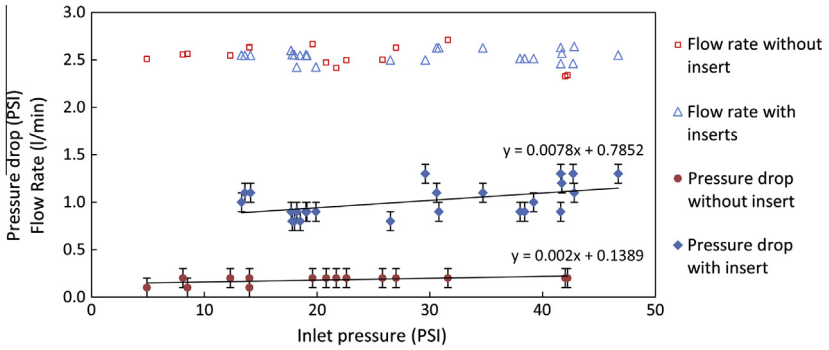

Fig. 12. Pressure drop in TEG40 with 8 mm panel insert and without insert.

3.5. Work due to increased pressure drop

It does not go unnoticed that the thermal enhancement benefits of the turbulating inserts come with an adverse rise in friction resulting in an increase in pressure drop subsequently adding work to maintain the flow rate. It is therefore necessary to quantify this added work brought upon by the turbulating inserts relative to the power production of the generator. In order to minimize the uncertainty in the pressure drop measurements with the available equipment for this study, the pressure drop is measured using the pipes of the Teg40 generator rather than the Teg8 generator. This is due to its relatively long channels resulting in a relatively large pressure drop thereby minimizing the percentage uncertainty in the measurements. Using the test stand described in Section 2.5, the pressure drop due to tubular flow in absence of any flow impeding obstacles and the pressure drop due to tubular flow when fitted with 8 mm Panel Inserts are compared. The results are presented in Fig. 12 in conjunction with the flow rate measurements in order to confirm that the flow rates are maintained at 2.5 ± 0.2 l/min for a mean pressure range of 5–45 PSI.

The results show that the pressure drop across the flow channels of the Teg40 in an absence of inserts is 0.18 ± 0.05 PSI per channel. When fitted with the 8 mm Panel Insert the pressure drop per channel is raised to an average of 1.01 PSI. From Eq. (3), the increase of pumping power needed to maintain the flow rate with the 8 mm Panel Inserts relative to an absence of inserts is 1.427 ± 0.41 W.

3.6. Net thermoelectric power enhancement

The thermoelectric power enhancement's ability to offset the added work due to the increased pressure drop in the presence of the 8 mm Panel Inserts is measured using the results obtained in Section 3.5. The net power enhancement using these flow turbulating inserts is defined as,

$$P^{+} = \frac{P_i - \dot{W}_{\Delta p}}{P_o} \tag{8}$$

in which $\dot{W}_{\Delta p}$ is the power increase necessary to maintain the flow rate in the presence of the insert relative to an absence of inserts. The net thermoelectric power enhancement of the TEG40 generator when using 8 mm Panel Inserts at 2.5 l/min flow rate per channel under varying thermal input conditions and its rate of change with respect to ΔT are illustrated in Fig. 13. It is important to note that a net power gain is attained for P^{+} values that are greater than unity. The $P^{+\prime}$ values represent the slope of the P^{+} curve effectively illustrating the sensibility of the net power gain to the thermal input conditions. More specifically, it is shown in Fig. 13 that although the net gain is less than unity for the lower range of thermal input conditions, its rate of change is positive and relatively large in this range implying relatively large gains in net power gain for increment increases in temperature. Furthermore, the rate of change of net power with respect to ΔT for the upper range of ΔT values is shown to remain positive for all thermal input conditions tested

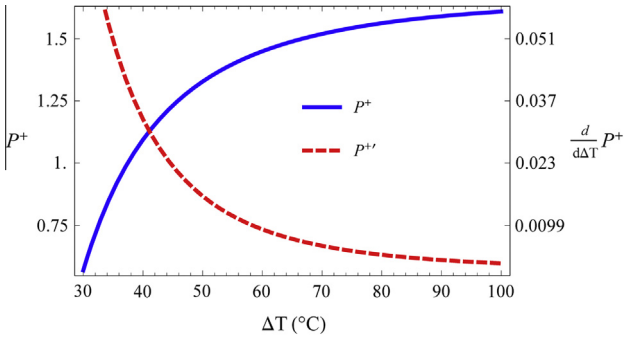

Fig. 13. Net thermoelectric power enhancement of TEG40 using 8 mm Panel inserts at 2.5 l/min per flow channel.

converging to a near zero constant implying relatively small increases in net power gain for increment increases in temperature.

The results of Fig. 13 demonstrate that the thermoelectric power enhancement begins to offset the increase pressure drop at a ΔT of 37 °C. For lower values, the 8 mm Panel Inserts for the tested generator under the given operating conditions do not enhance the power sufficiently to justify their use. Furthermore, the instantaneous rate of change evolution curve shows that the net power gains increase sharply with an increasing thermal dipole at lower temperatures transitioning to less significant gains at higher temperatures. This is noteworthy since, in this study, the 8 mm Panel Inserts create a velocity profile which, relative to other inserts tested, produces the greatest thermal enhancement and subsequently the greatest power improvement at all temperatures.

The results elucidate the importance of identifying the most appropriate turbulating inserts for an application's target temperature range.

4. Conclusion

A reliable test stand is built to measure the thermoelectric power enhancement of a liquid-to-liquid thermoelectric generator when its flow channels are fitted with turbulating inserts of three different geometric shapes. It is shown that the Spiral Inserts produce negligible power enhancement and that the Panel Inserts enhance power up to 110%. Thermoelectric power enhancement is attributed to velocity field alterations brought upon by the inserts. In particular, the thermal enhancement factor of each test case is measured illustrating that the power enhancement is due to an increase in heat transfer rate at the channel walls. Numerical simulations of the internal channel velocity field demonstrate that the thermal enhancement is attributed to the field synergy principle implying that the angle between the velocity vector and the temperature gradient is reduced in the presence of Panel Inserts. More specifically, the Spiral inserts are shown to produced a mean velocity field profile which mirrors that of the fully developed internal pipe flow thereby minimally altering the thermal transport. In contrast, the Panel inserts are shown to effectively invert the mean velocity profile such that its local maximum is closer to the channel wall than the central axis thereby improving the thermal transport at the periphery of the flow pipes. Furthermore, for the tested operating conditions of this study, the results show that while Panel Inserts provide greater thermoelectric power enhancement than Spiral Inserts, doubling the number of panels on the Panel Inserts has a negligible effect on the power improvement.

The increase in pressure drop due to the presence of Panel Inserts is measured relative to an absence of inserts in order to evaluate the power enhancement necessary to offset the power needed to maintain the flow rate. For the largest tested generator containing 40 thermoelectric modules, the power enhancement due to the presence of Panel Inserts offsets the adverse increase in pressure drop for ΔT values of 37 °C and greater. For greater ΔT values the net thermoelectric power enhancement is positive and the net gain continues to increase with respect to temperature reaching more than a 50% net gain relative to an absence of inserts beyond ΔT = 70 °C. The results demonstrate that proper use of turbulating inserts for thermoelectric power enhancement is dependant of the target thermal input conditions of the application.

Acknowledgments

The authors thank Marc Désaulniers, Kruger Products, Gerard Campeau of Thermoelectronics Corp. and the Fondation du Cégep de l'Outaouais for their valuable support throughout this project. The authors also gratefully acknowledge the technical expertise of Rémi Pelletier and Stéphane Piché.

References

[1] Rowe DM. Thermoelectrics handbook macro to nano. Taylor & Francis, Group; 2006.
[2] André C, Vasilevskiy D, Turenne S, Masut RA. Extruded bismuth–telluride-based n-type alloys for waste heat thermoelectric recovery applications. J Electron Mater 2009;38:1061–7.
[3] Poudeu PFP, Guéguen A, Wu C-I, Hogan T, Kanatzidis MG. High Figure of Merit in nanostructured n-type HPb_mSbTe_{m+2} thermoelectric materials. Chem Mater 2010;22:1046–53.
[4] Ebling D, Bartholomé K, Bartel M, Jägle M. Module geometry and contact resistance of thermoelectric generators analyzed by multiphysics simulation. J Electron Mater 2010;39:1376–80.
[5] Hadjistassou C, Kyriakides E, Georgiou J. Designing high efficiency segmented thermoelectric generators. Energy Convers Manage 2013;66:165–72.
[6] Gou X, Xiao H, Yang S. Modeling, experimental study and optimization on low temperature waste heat thermoelectric generator system. Appl Energy 2010;87:3131–6.
[7] Wee D. Analysis of thermoelectric energy conversion efficiency with linear and nonlinear temperature dependence in material properties. Energy Convers Manage 2012;52:3383–90.
[8] Bélanger S, Gosselin L. Thermoelectric generator sandwiched in a crossflow heat exchanger with optimal connectivity between modules. Energy Convers Manage 2012;52:2911–8.
[9] Crane DT, Jackson GS. Optimization of cross flow heat exchangers for thermoelectric waste heat recovery. Energy Convers Manage 2004;45:1565–82.
[10] Rodriguez A, Vian JG, Astrain D, Martinez A. Study of thermoelectric systems applied to electric power generation. Energy Convers Manage 2009;50:1236–43.
[11] Whalena SA, Dykhuizenb RC. Thermoelectric energy harvesting from diurnal heat flow in the upper soil layer. Energy Convers Manage 2012;64:397–402.
[12] Karabetoglu S, Sisman A, Faith Ozturk Z, Sahin T. Characterization of a thermoelectric generator at low temperatures. Energy Convers Manage 2012;62:47–50.
[13] Hsiao YY, Chang WC, Chen SL. A mathematic model of thermoelectric module with applications on waste heat recovery from automobile engine. Energy 2010;35:1447–54.
[14] Zhang X, Chau KT. An automotive thermoelectric–photovoltaic hybrid energy system using maximum power point tracking. Energy Convers Manage 2011;52:641–7.
[15] Karri MA, Thacher EF, Helenbrook BT. Exhaust energy conversion by thermoelectric generator: two case studies. Energy Convers Manage 2011;52:1596–611.
[16] Hsu C-T, Huang G-Y, Chu H-S, Yu B, Yao D-J. Experiments and simulations on low-temperature waste heat harvesting system by thermoelectric power generators. Appl Energy 2011;88:1291–7.
[17] Love ND, Szybist JP, Sluder CS. Effect of heat exchanger material and fouling on thermoelectric exhaust heat recovery. Appl Energy 2012;89:322–8.
[18] O'Shaughnessy SM, Deasy MJ, Kinsella CE, Doyle JV, Robinson AJ. Small scale electricity generation from a portable biomass cookstove: prototype design and preliminary results. Appl Energy 2013;102:374–85.
[19] Xiao J, Yang T, Li P, Zhai P, Zhang Q. Thermal design and management for performance optimization of solar thermoelectric generator. Appl Energy 2011;93:33–8.
[20] Goldsmid HJ, Giutronich JE, Kaila MM. Solar thermoelectric generation using bismuth telluride alloys. Solar Energy 1980;24:435–40.
[21] He W, Su Y, Wang YQ, Riffat SB, Ji J. A study on incorporation of thermoelectric modules with evacuated-tube heat-pipe solar collectors. Renew Energy 2012;37:142–9.
[22] Lesage FJ, Pelletier R, Fournier L, Sempels E. Optimal electrical load for peak power of a thermoelectric module with a solar electric application. Energy Convers Manage 2013;74:51–9.
[23] Chávez-Urbiola EA, Vorobiev YuV, Bulat LP. Solar hybrid systems with thermoelectric generators. Solar Energy 2012;86:369–78.
[24] Deng Y, Zhu W, Wang Y, Shi Y. Enhanced performance of solar-driven photovoltaic–thermoelectric hybrid system in an integrated design. Solar Energy 2013;88:182–91.
[25] Palma P, Pérez-Aparicio JL, Bravo R. Study of hysteretic thermoelectric behaviour in photovoltaic materials using the finite method, extended thermodynamics and inverse problems. Energy Convers Manage 2013;65:557–63.
[26] Stevens JW. Optimal design of small ΔT thermoelectric generation systems. Energy Convers Manage 2001;42:709–20.
[27] Yu C, Chau KT. Thermoelectric automotive waste heat energy recovery using maximum power point tracking. Energy Convers Manage 2009;50:1506–12.
[28] Miller EW, Hendricks TJ, Peterson RB. Modeling energy recovery using thermoelectric conversion integrated with an organic rankine bottoming cycle. J Electron Mater 2009;38:1206–13.
[29] Dai D, Zhou Y, Liu J. Liquid metal based thermoelectric generation system for waste heat recovery. Renew Energy 2011;36:3530–6.

[30] Kristiansen NR, Snyder GJ, Nielsen HK, Rosendahl L. Waste heat recovery from a marine waste incinerator using a thermoelectric generator. J Electron Mater 2012;41:1024–9.
[31] Hendricks TJ, Karri NK, Hogan TP, Cauchy CJ. New perspectives in thermoelectric energy recovery system design optimization. J Electron Mater 2013:1–12.
[32] Lesage FJ, Pagé-Potvin N. Experimental analysis of peak power output of a thermoelectric liquid-to-liquid generator under an increasing electrical load resistance. Energy Convers Manage 2013;66:98–105.
[33] Hodes M. On one-dimensional analysis of thermoelectric modules [TEMs]. IEEE Trans Comp Pack Technol 2005;28:218–29.
[34] Promvonge P, Chompookham T, Kwankaomeng S, Thianpon C. Enhanced heat transfer in a triangular ribbed channel with longitudinal vortex generators. Energy Convers Manage 2010;51:1242–9.
[35] Jaisankar S, Radhakrishnan TK, Sheeba KN. Experimental studies on heat transfer and thermal performance characteristics of thermosyphon solar water heating with helical and left–right twisted tapes. Energy Convers Manage 2011;52:2048–55.
[36] Incropera, FP, Dewitt DP, Bergman TL, Lavine AS. Introduction to heat transfer. 5th ed. John Wiley and Sons; 2007.
[37] Tijing LD, Pak BC, Baek BJ, Lee DH. A study on heat transfer enhancement using straight and twisted internal fin inserts. Int Commun Heat Mass Transfer 2006;33:719–26.
[38] Guo ZY, Li DY, Wang BX. A novel concept for convective heat transfer enhancement. Int J Heat Mass Transfer 1998;41:2221–5.
[39] Cai R, Gou C. Discussion on the convective heat transfer and field synergy principle. Int J Heat Mass Transfer 2007;50:5168–76.
[40] Ma LD, Li Z-Y, Tao W-Q. Experimental verification of the field synergy principle. Int Commun Heat Mass Transfer 2007;34:269–76.
[41] Kuo J-K, Yen T-S, Chen C-K. Improvement of performance of gas flow channel in PEM fuel cells. Energy Convers Manage 2008;49:2776–87.
[42] Jones WP, Launder BE. The prediction of laminarization with a two-equation model of turbulence. Int J Heat Mass Transfer 1972;15:301–14.